Biophysical evidence that frostbite is triggered on nanocrystals of biogenic magnetite in garlic cloves (*Allium sativum*)

Check for updates

Atsuko Kobayashi [1,2,3] ✉, Daisuke Tanaka [4,5] ✉, Hironori Hidaka [6], Kasumi Sakurai [7], Kotaro Kawai[7], Toyohiro Kato[7], Kumiko Kihara[8] & Joseph L. Kirschvink [1,2,3] ✉

Trace levels of biologically precipitated magnetite (Fe_3O_4) nanocrystals are present in the tissues of many living organisms, including those of plants. Recent work has also shown that magnetite nanoparticles are powerful ice nucleation particles (INPs) that can initiate heterogeneous freezing in supercooled water just below the normal melting temperature. Hence there is a strong possibility that magnetite in plant tissues might be an agent responsible for triggering frost damage, even though the biological role of magnetite in plants is not understood. To test this hypothesis, we investigated supercooling and freezing mortality in cloves of garlic (*Allium sativum*), a species which is known to have moderate frost resistance. Using superconducting magnetometry, we detected large numbers of magnetite INPs within individual cloves. Oscillating magnetic fields designed to torque magnetite crystals in situ and disturb the ice nucleating process produced significant effects on the temperature distribution of supercooling, thereby confirming magnetite's role as an INP in vivo. However, weak oscillating fields increased the probability of freezing, whereas stronger fields decreased it, a result that predicts the presence of magnetite binding agents that are loosely attached to the ice nucleating sites on the magnetite crystals.

Since the end of the last global glaciation (Snowball Earth) event 635 million years ago[1], Earth's climate has fluctuated between 'Ice-House' intervals with polar ice caps and 'Greenhouse' intervals with overall clement conditions[2]. Each glacial interval consisted of numerous shorter-duration glacial/interglacial advance and retreat cycles driven by variations in Earth's orbit. As the earliest known embryophyte land plants date to mid-Ordovician time[3] (~470 million years ago), there have been numerous glacial advance and retreat cycles during which mid to high-latitude land plants needed to adapt to seasonal freezing events.

Despite the long intervals of geological time that plants have had to adapt to cold conditions, not all have done so[4]. As a consequence, frost damage in plants is a significant contributor to agricultural losses[5,6]. Understanding how the basic physical systems work that have evolved to control ice crystal formation in living tissues is therefore important, as this knowledge could help to improve the human food supply.

Past studies of cold tolerance have revealed a complex variety of cold adaptations, allowing some plants, such as trees in the aboral forests, to survive winter temperatures as low as −50 °C[4]. Survival at these temperatures requires careful activation of genetic control systems via stepwise pre-freezing temperature drops which mimic the cooling steps of Autumn, leading into the Winter months. Antifreeze compounds that are synthesized vary greatly among cold-adapted species but are known to include solutes such as amino acids and sugars that depress the freezing point, and several proteins and other hydrocarbons that either inhibit ice nucleation or block ice crystal propagation[7]. In particular, supercooling (the retention of a liquid state at temperatures below the melting point) is an important adaptation used by numerous plants to avoid freezing[4] in sub-zero weather.

In water, supercooling can only be achieved in the absence of ice crystal seed nuclei. Seed crystals nucleate either through heterogeneous or homogeneous processes. Homogeneous ice nucleation typically happens at

[1]Earth-Life Science Institute, Tokyo Institute of Technology, Meguro, Tokyo, Japan. [2]Division of Geological & Planetary Sciences, California Institute of Technology, Pasadena, CA, USA. [3]Marine Core Research Institute, Kochi University, Nankoku, Kochi, Japan. [4]Research Center of Genetic Resources, National Agriculture and Food Research Organization, Tsukuba, Ibaraki, Japan. [5]Institute of Life and Environmental Sciences, University of Tsukuba, Ibaraki, Japan. [6]Department of System and Control Engineering, School of Engineering, Tokyo Institute of Technology, Meguro, Tokyo, Japan. [7]Department of Mechanical Engineering, School of Engineering, Tokyo Institute of Technology, Meguro, Tokyo, Japan. [8]Department of Biological and Chemical Systems Engineering, National Institute of Technology, Kumamoto College, Kumamoto, Japan. ✉e-mail: atsuko.kobayashi@kochi-u.ac.jp; dtanaka@affrc.go.jp; kirschvink@caltech.edu

temperatures of −30 °C and below and involves a cluster of several hundred molecules that transiently arrange themselves into a seed crystal, leading to the rapid crystallization of the surrounding, supercooled liquid[8]. However, water can freeze at higher temperatures through the heterogeneous nucleation process, in which a mineral or other substrate is present with a surface charge distribution that helps to organize the water molecules into the hexagonal arrangement for ice. If such ice nucleating particles (INPs) are absent, water in plant tissues can often remain liquid down to the homogenous freezing limit. Minerals are volumetrically rare in most plant (and animal) tissues[9], but if an INP is present even in minute concentrations somewhere in the tissue that acts at temperatures closer to the melting point, it can form an ice crystal that will rapidly propagate throughout the contiguous liquid volume.

Over the past 80 years, materials discovered to be efficient at heterogeneous ice nucleation include the silver iodide crystals used for seeding clouds[10], proteins from cryogenically-adapted animals and bacteria (sometimes used to inhibit freezing in foods[11]), as well as minerals like feldspars[12] which are present in the Eolian dust which is important for cloud formation. Kobayashi et al. [13] recently found that supercooling is nearly eliminated by trace levels (ng/g) of magnetite nanocrystals (Fe_3O_4) dispersed in ultrapure water, showing that it is also a powerful INP[13,14].

Magnetite particles >∼30 nm in size can be detected with exquisite sensitivity (∼1 part in 10^{12}) using superconducting quantum interference devices (SQUIDs) configured as moment magnetometers[15]. These particles are above the superparamagnetic to single-domain size threshold and are, therefore, stably (permanently) magnetized[16]. Torques from external magnetic fields can, therefore, act to physically rotate the magnetite crystals, rather than simply deflecting their magnetic moments without physically rotating the crystals (as happens in the smaller, superparamagnetic particles). Nanoparticles of magnetite dispersed in fluids will act like tiny compass needles, aligning with the local magnetic field following the relatively simple physics of viscously damped, torque-driven rotations where the torque (τ) is the vector cross-product of the time-varying magnetic field (B) with the particle's magnetic moment (μ)[17], or

$$\tau = \mu \times B \quad (1)$$

Note that a full discussion of the equation of motion, including the coefficient of rotational friction, is given in ref. 17. Similarly, the magnetostatic potential energy, E, of the system is given by the vector dot-product

$$E = -\mu \cdot B \quad (2)$$

As noted below, the energy per magnetite nanoparticle can be several thousand times that of the background thermal noise for magnetic fields only one to two orders of magnitude stronger than that of the Earth. Generating turbulence at the surface of in vitro magnetite nanoparticles by driving them with inclined, rotating magnetic fields acts to inhibit ice crystal nucleation with negligible local heating[17]. No other biophysical mechanism is known that can affect ice crystal nucleation via low-intensity (10× Earth strength), low-frequency (∼10 Hz) magnetic fields[14,18].

Numerous studies of animal tissues using the SQUID moment magnetometers show that magnetite is present typically in concentrations in the 10–100 ng/g range, with crystal morphologies and ultrastructural arrangements in magnetic extracts indicating that they are biologically-controlled, in-situ mineral precipitates[19–21]. Some of these are similar to the strings of membrane-bound magnetosomes found in numerous magnetotactic microorganisms[22,23]. Plants are also known to have biogenic magnetite. An earlier report of magnetite of superparamagnetic size in grasses[24] was followed by magnetometry-based detection of single-domain magnetite in a variety of common garden species[25]. Recently, Goroberts et al.[26] presented images of classical magnetosome chains in the walls of the sieve tubes of the phloem in tobacco and potato tissues[26].

For our studies, we wanted to investigate the possible role of magnetite as INPs in plants, using a species that could supercool to moderate temperatures on the order of ∼−10 °C. We chose garlic because James et al.[27] demonstrated that whole cloves (*Allium sativum*) will supercool down to as cold as −13 °C, well below its melting temperature of −2.7 °C. Garlic is a ground bulb that grows in environments periodically subjected to freezing conditions during the winter months[28,29], and hence may have evolved mechanisms to inhibit any INPs that might be present.

Using clean-lab-based SQUID moment magnetometry, as noted below, we detected the presence of large numbers of magnetite nanocrystals within individual garlic cloves, with rock-magnetic properties indicating that they should normally act as INPs and initiate freezing slightly below 0 °C. We then tested the freezing-survivorship effect of the 10 Hz rotating magnetic fields at 4 levels (up to ∼50 times stronger than the Earth's magnetic field) that were able to suppress freezing in magnetite-spiked water[17] on garlic cloves subjected to background temperatures between −9.5 and −15 °C.

We report here that the supercooled/freezing transition is associated strongly with loss of viability ($p \ll 0.001$). Rotating magnetic fields, designed to oscillate the magnetite nanocrystals, had significant effects on the supercooling trajectories, confirming that magnetite is indeed an INP in this system. However, compared with sham controls, the magnetic exposures increased the freezing probability below 1.5 mT but depressed it at field strengths of 2 mT and higher. Our results can be explained by the presence of surface binding substances that inhibit heterogeneous ice nucleation on magnetic particles in garlic cloves; similar agents have been identified that block crystal growth sites directly on ice crystals[30]. If such agents are attached weakly to the magnetite crystal surfaces, weak oscillating magnetic fields should be able to dislodge them, initially increasing the freezing probability and inhibiting supercooling. Stronger oscillations would then inhibit ice nucleation by directly disrupting the incipient water clusters, lowering the supercooling temperature. Surface-binding moieties of this sort are potential biotechnology targets.

Results

A total of 721 individual garlic cloves from 127 bulbs were subjected to cooling experiments in the apparatus shown in Fig. 1. Important data include tabulations of the magnetic exposure conditions (Field levels vs. Shams), the lowest temperature individual cloves reached before freezing events (if any), the equilibrium temperature for the bulbs at the end of the experiment, and the post-experimental viability checks (Living vs. Dead). We first discuss the simple categorical results of the numbers of the cloves that survived (or died) vs. the magnetic (or sham) treatments. This is followed by the analysis of the survivorship curves within these groups as a function of the measured cooling temperatures.

Survival vs. magnetic exposure experiments

All 721 cloves that were assayed for viability (Living vs. Dead) were previously exposed to either a 10 Hz processing magnetic field at one of 4 intensities or experienced a paired sham condition (see the "Methods" section). This forms a set of 2 × 2 contingency tables (Alive/Dead vs. Field/Sham), with 4 exposure levels (1.0, 1.5, 2.0, and 2.5 mT). Table 1 shows the resulting data, broken down first from the group of all field settings to an intermediate split of low and high fields (≤1.5 and ≥2.0 mT), and then to the individual exposure levels. The combined data set shows a significant increase in survival of about 8%. However, when split into the high and low categories, the low-field set is not significant, whereas the high category (≥2.0 mT) shows a highly significant 17% increase. Further subdivision to the individual categories shows that the 1.0 mT group has a significant 9% *decrease* in survival from field exposure, compared with significant *increases* of 14%, 17%, and 24% survival rates for the higher field groups. The Cochran–Mantel–Haenszel test of independence for repeated 2 × 2 contingencies (see the "Methods" section) also confirms the rejection of the null hypothesis of no consistent differences.

Magnetic supercooling experiments

Figure 2 shows a typical example of the thermal recordings of a garlic bulb with six of the eight thermocouples taped to the outside of individual cloves,
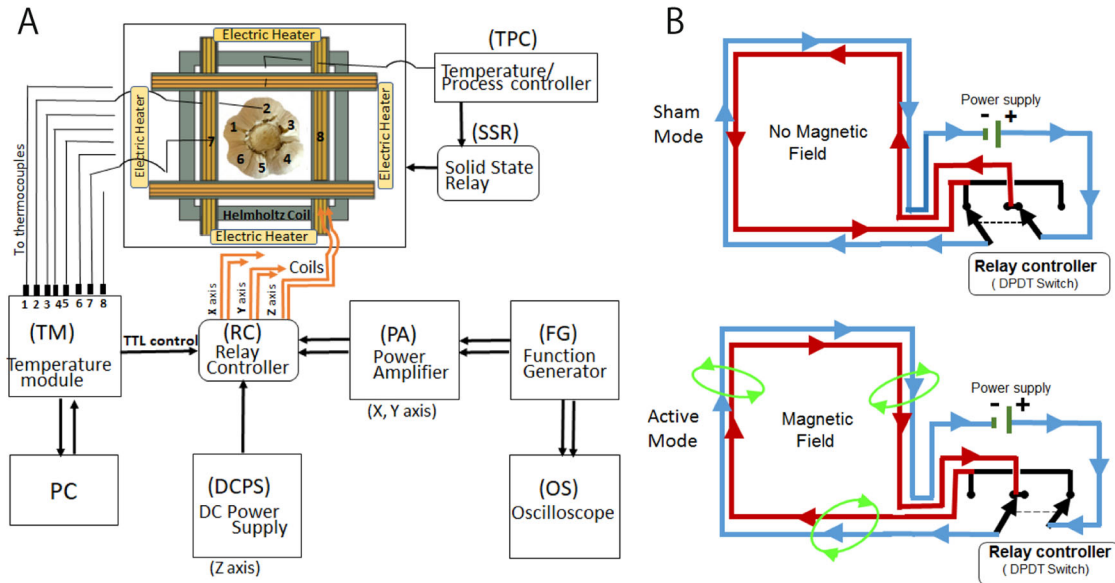
Fig. 1 | Schematic diagrams of the experimental apparatus used in these experiments. A A Styrofoam box similar to that described by Kobayashi et al.[17] was supported by wooden blocks inside a −80 °C refrigerator. The desired equilibrium temperature was maintained via an external temperature process controller which was monitoring the bottom center of the box with a thermocouple, warming the system with electric heating pads if it fell below the chosen setpoint. Rotating magnetic fields were generated with a set of 3-axis square Helmholtz coils, driven in the horizontal plane by a 2-channel audio power amplifier. Other devices are as described in the "Methods" section. **B** Coil wiring schematic diagram, which allows the setting of experimental conditions that are fully active or active-sham. All three coil sets were double-wrapped, allowing double-pole, double-throw (DPDT) relays to reverse the current flow in one of the windings. The top diagram shows the configuration where the currents are antiparallel, canceling external fields for the "Sham" settings. The bottom shows the switch configuration with the current flowing in parallel, generating the external fields for this experiment.

Table 1 | Categorical 3-way contingency tests for the garlic freezing experiments, comparing field exposures with the living vs. dead assays made following the exposures

Field level (mT)	Setting	Survival?		Total:	% Alive	Live–dead comparison (%)	χ^2	*p*-value	Significance & notes
		Alive	Dead						
All levels	Field	211	159	370	57	8	5.34	0.021	Field increases survival
	Sham	170	181	351	48				
	Total	381	340	721					
≤1.5 mT	Field	122	66	188	65	1	0.02	0.898	n.s., Effects cancel out
	Sham	106	59	165	64				
≥2.0 mT	Field	89	93	182	49	17	7.95	0.005	Field increases survival
	Sham	64	122	186	34				
	Total	381	340	721					
1.0	Field	66	34	100	66	−9	4.32	0.038	Field decreases survival
	Sham	67	17	84	80				
1.5	Field	56	32	88	64	14	4.11	0.043	Field increases survival
	Sham	39	42	81	48				
2.0	Field	51	37	88	58	17	5.42	0.020	Field increases survival
	Sham	45	64	109	41				
2.5	Field	38	56	94	40	24	4.73	0.030	Field increases survival
	Sham	19	58	77	25				
	Total	381	340	721					
Cochran–Mantel–Haenszel test for repeated 2 × 2 tests of independence							5.47	0.019	Reject hypothesis of consistent differences

Field levels are in milliTesla (mT), paired with their respective sham groups. Results of Pearson's[50] χ^2 test of independence are shown for each category, along with the associated *p*-values. (n.b.: Two-tailed significance levels in this paper are indicated as follows: significant is $p < 0.05$; highly significant is $p < 0.01$; and very highly significant is $p < 0.001$; n.s. is not significant). The live–dead comparison is given by the ratio (%Alive − %Dead)/(%Alive + %Dead). The surprising result is that the weakest field exposure level significantly *reduces* the fraction surviving, whereas the stronger fields significantly *increase* the survival probability.

and the other two recording the background temperature in the chamber for up to 20 h (see the "Methods" section). Ice nucleation (freezing) events are clearly visible from the temperature spikes, wherein the supercooled water within a garlic clove releases the latent heat of crystallization for water (~80 calories/g). Small thermal anomalies are sometimes visible on other sensors mounted on the bulb, reflecting a mild rise in ambient temperature from the

Fig. 2 | Typical plot of the thermocouple recordings made with the cooling system (described in the "Methods" section). The garlic bulbs were approximately at room temperature when thermocouples #1 to #6 were attached to the surface of individual cloves. Over the course of the first one to two hours they equilibrate with the background temperature as shown. Thermocouples #7 and #8 remained in the freezing chamber and recorded a brief transient warming as the background air was heated slightly from the introduction of a room-temperature garlic bulb. Abrupt jumps in the temperature with a sharp peak indicate a freezing event in the adjacent clove. Overlapping bumps are presumably the result of heat dissipating from a single clove warming adjacent ones.

Table 2 | χ^2 test of independence[50] between the presence of a freezing spike and viability

	Alive	Dead	Total
Frozen	9	277	286
Unfrozen	243	14	257
Total	252	291	543
χ^2	455	$p < 0.001$	

The null hypothesis that the freezing and survival are independent of each other is rejected with very high confidence. The observed freezing spikes are associated with death.

heat pulse released by the freezing event in an adjacent clove. In this example, three of the garlic cloves in the bulb (#2, #3, and #5) experienced freezing events and did not survive. The other three (#1, #4, and #6) did not freeze and were subsequently found to be viable.
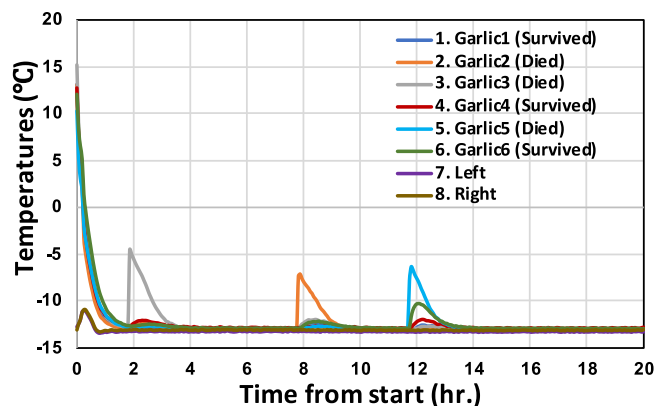
Viability, supercooling, and magnetic field exposure

An important question concerns whether ice crystal growth, indicated by the thermal spikes from the end of the supercooling, is associated with subsequent viability. Table 2 shows the results from a χ^2 test of independence for the categories Alive/Dead vs. Frozen/Unfrozen for the 543 garlic cloves in our experiments that had direct thermocouple recordings showing the presence or absence of a freezing spike, and which were assayed for subsequent viability. The χ^2 value is 455 ($p < 0.001$), allowing us to reject with very high confidence the null hypothesis that freezing and survival are not related. The fraction of observed unfrozen but dead cloves (14 out of 257, or ~5%) seems slightly higher than the low levels reported for this cultivar strain by the farmers utilizing it. Although as yet unquantified, this might indicate some slight increase in mortality from supercooling. A similarly small fraction of cloves that did freeze were still viable, perhaps implying that the germinal cells sometimes can avoid the fatal effect of the crystallizing ice.

Magnetic effects on survivorship

Figure 3 and Table 3 show the results of the Kaplan–Meier[31] analyses of survivorship. Numerical source data are in Supplemental Data 1. As shown in Fig. 3A, the 1 mT oscillating field significantly increased the freezing probability compared to the shams, contrary to our prior expectations that oscillating fields should inhibit ice nucleation[17], but in agreement with the overall contingency test analysis shown in Table 1. In the 1.5 mT level group shown in Fig. 3B, this tendency continues down to about −12.5 °C, below which the two curves cross and the field exposed group does better. Finally, in fields ≥2.0 mT the field-exposed group does significantly better than the sham controls throughout the entire temperature spectrum (Fig. 3C), which also agrees with the contingency test results. Individual distributions with 95% confidence intervals are shown in Supplementary Fig. 1.

Rock magnetic results

Mineralogical and particle size constraints in Fig. 4B, C are provided by the magnetic coercivity spectral analysis shown in Fig. 4A, via the paired demagnetization and magnetization of the isothermal remanent magnetization (IRM). Numerical source data used for Fig. 4A are in Supplemental Data 1. Elongate magnetite needles have a maximum coercivity of 300 mT, with their oxidized topotactic equivalent maghemite (γ-Fe$_2$O$_3$) having slightly higher values. As all curves flatten out above 300 mT, the mineral is most likely ferrimagnetic, like magnetite/maghemite, rather than anti-ferromagnetic minerals like hematite or goethite[32]. Data shown in
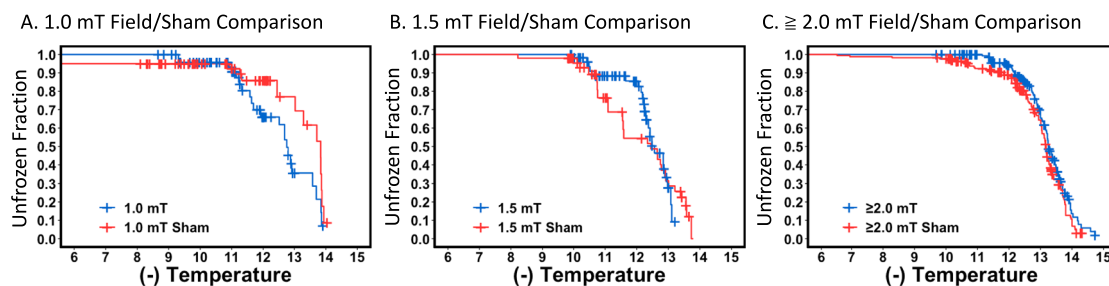

Fig. 3 | Survivorship analysis of freezing events vs. temperature decrease. As described in the "Methods" subsection "Survivorship statistics", we follow a modified Kaplan and Meier[31] survivorship analysis to estimate the freezing probability with cooling. For this we treat freezing (≅death) as a function of decreasing temperature ($-T$), rather than with time because James et al.[27] found temperature was the dominant parameter controlling freezing in supercooled garlic cloves. A–C respectively show the fraction of unfrozen cloves as a function of the (−) temperature from the experiments. Blue curves show the results of the field exposure experiments, and red shows the corresponding shams. Tick marks indicate data that were Right-censored, as discussed in Methods. Statistical results are given in Table 3. Data for the 1.0 mT comparison shows that the magnetic exposure significantly enhances the probability of freezing. At 1.5 mT the magnetic exposure appears to *inhibit* freezing slightly below about −12.5 °C, then the curves cross with a slight inhibition at the lower temperatures. In stronger fields the magnetic exposure significantly inhibits freezing relative to the controls at all temperatures.

Table 3 | Statistical results of supercooling temperature as a function of magnetic field strength, as described in the "Methods" section, for the groups shown in Fig. 3

Treatment		Total # analyzed	# Exactly observed	# Right censored	Mann–Whitney–Wilcoxon test (2-tailed Wilcoxon rank-sum test)			
					Z value	*n* score	*p*-value	Comment
A. 1.0 mT	Field	91	21	70	2.061	+4.245	0.039	Field-treated freezes before sham
	Sham	79	12	67				
B. 1.5 mT	Field	80	22	58	−0.434	−1.065	0.664	Indeterminate
	Sham	66	25	41				
C. ≥2.0 mT	Field	175	90	85	−2.020	-9.345	0.043	Field-treated freezes after sham
	Sham	180	116	64				

Field and sham experiments at a given current level were done using garlic bulbs from the same allocation to reduce the variability that might arise from uncontrolled factors such as age and magnetite content. Out of the 721 garlic cloves examined, there were 543 total cloves measured with thermocouples (Supplementary Data 1), of which 286 froze (Exactly Observed) according to the thermocouple spikes. The rest were censored as described in the "Methods" section. Use of the Wilcoxon test rather than a Log-Rank test is appropriate here because the probability of ice nucleation events is not constant with temperature[57] (see ref. 53 for a discussion on the statistics).
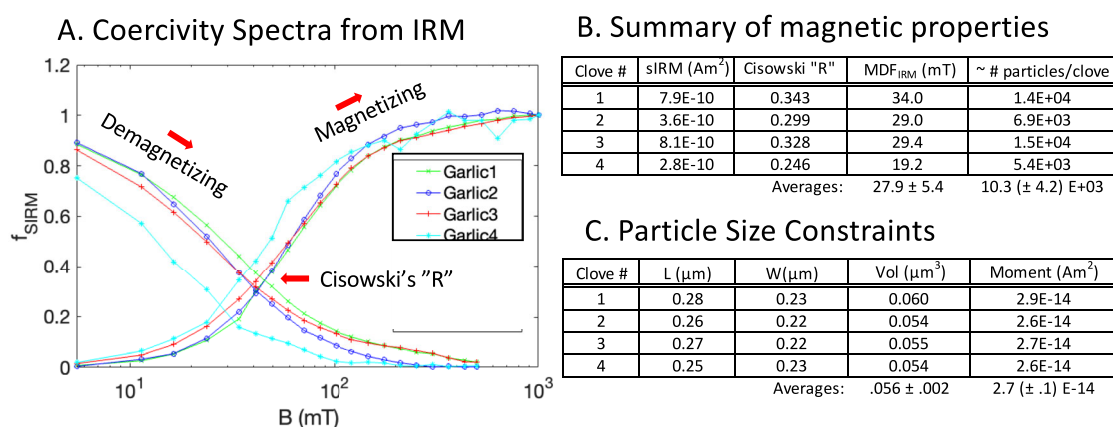

Fig. 4 | Rock-magnetic constraints on the micro-granulometry of magnetite in garlic cloves. **A** Coercivity spectra determinations based on the progressive acquisition and demagnetization of the IRM, for the individual garlic cloves. Cisowski's "*R*" value is the *Y*-axis coordinate of the intersection of the paired magnetizing and demagnetizing curves for each sample. The corresponding *X*-coordinate is the median destructive field (MDF$_{IRM}$). **B** Summary of magnetic properties, including saturation IRM (sIRM), the maximum remanent magnetization after exposure to an ~1 T single pulse, the Cisowski intersection "*R*", and the microscopic coercivities (MDF$_{IRM}$ values) from the data of (**A**). **C** Results tabulated in terms of a right elliptical solid. The magnetic moment of these average crystals is determined directly from this volume from the saturation magnetization (see the "Methods" section). Finally, the average moment per crystal constrains the number of particles per garlic clove, as tabulated in (**B**).

Supplementary Fig. 2 constrains the average crystals to be of single-domain size, arranged in clumps of moderately interacting particles. As shown in Fig. 4B, C, Cisowski's "*R*" value of interaction is depressed from its maximum value of 0.5 for randomly oriented non-interacting single domains, indicating that interparticle interactions are depressing this value from this theoretical maximum by aiding the demagnetization, and inhibiting the magnetization[33]. The MDF$_{IRM}$ values, in turn, constrain the average particle sizes expected for single-domain magnetite ellipsoidal solids, assuming the most equant morphology capable of yielding this coercivity. The length (*L*) and width (*W*) of these most equant grains of magnetite can be semi-quantitatively determined from Fig. 3 of Diaz-Ricci and Kirschvink[34]. The average coercivity values (MDF$_{IRM}$) also constrain the average crystal volume and the crystal magnetic moments as tabulated in Fig. 4B, C. In turn, the sIRM values coupled with the crystal magnetic moments indicate the presence of ~10,000 such particles per garlic clove.

Data for the acquisition of the anhysteretic remanent magnetization (ARM) shown in Supplementary Fig. 2A indicate that the magnetic domains in the garlic cloves are not arranged in linear chains like they are in the magnetotactic bacteria; the particles are in aggregations more akin to those in the radular teeth of the *Polyplacophoran* mollusks (the chitons), but in much smaller clumps. The Lowrie–Fuller test results shown in Supplementary Fig. 2B, where the coercivity of the ARM is higher than the IRM for all cloves, demonstrate that the remanent magnetization is dominated by single-domain (uniformly magnetized) crystals, also with significant interparticle interactions[35,36]. Finally, the warming of a 5 T sIRM applied to a zero-field cooled garlic clove described in Supplementary Fig. 3 shows the characteristic Verwey transition superimposed upon a background apparently dominated by trace levels of ferritin and aqueous diamagnetism, confirming that the ferromagnetic mineral is most likely a slightly oxidized magnetite.

Discussion

Our results provide evidence that weak magnetic fields designed to physically rotate single-domain magnetite nanoparticles can influence supercooling and survival in plants. Our data also demonstrate that it is indeed the sudden nucleation of ice and/or the resultant pulsed release of the latent heat of crystallization that kills the cells and ends viability (Table 2). Spectral recordings of the vibrations in the experimental apparatus indicate that the noise difference between the field/sham conditions (in both the horizontal and vertical orientations) are below the background acceleration experienced in the laboratory (see Supplementary Fig. 4) and are not responsible for these magnetic effects.

It is puzzling, however, that the results of the magnetic exposure did not follow the pattern predicted by our earlier work on synthetic magnetite dispersed in ultrapure water[13,17]. We expected to find a simple progressive decrease in the temperature of freezing with increasing magnetic torque on the magnetite nanoparticles, being limited by the temperature below which

A. Sham

A1

A2

B. Weak Field

B1

B2

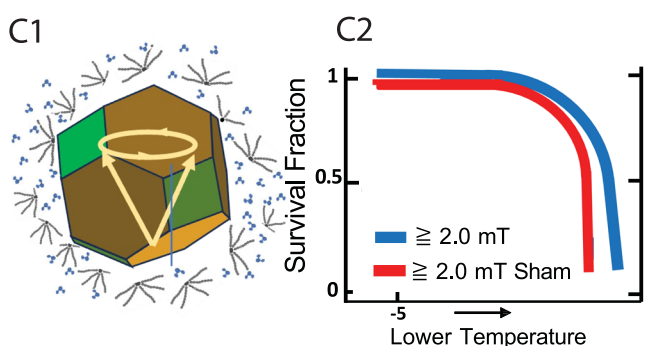## C. Strong Field

C1

C2
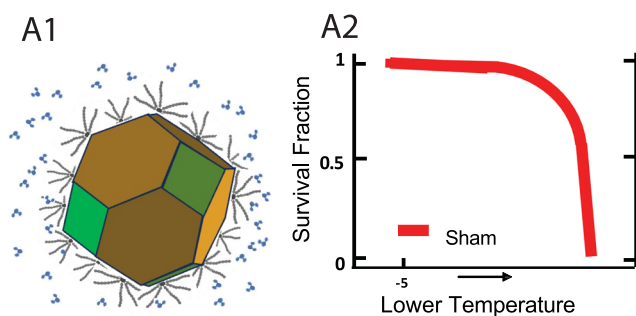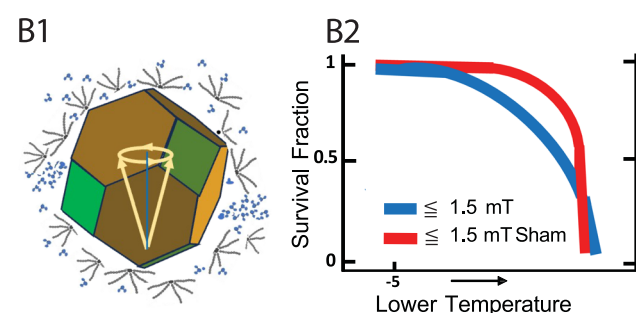
Fig. 5 | Schematic representation of how a progressively stronger magnetic agitation could first promote, then inhibit, ice nucleation on magnetite nanoparticles. A Sham situation. **A1** Binding agents (shown as radiating filaments) cover the particle surface as normal, blocking access to water molecules (three-dot objects). **A2** Sham reference curve (same in **B2** and **C2**). **B** Weak field situation. **B1** Surface binding agents are disrupted, allowing water molecules access to the crystal surface where ice crystals can nucleate, reducing the supercooling. Oscillations are not strong enough to disrupt ice seed crystals from nucleating. **B2** Garlic cloves exposed to this field freeze more easily than the controls, as illustrated by the blue curve lying to the left of the sham control curve. **C** Strong field situation. **C1** Both the binding agent and the water molecules are driven away from the crystal surface. **C2** The magnetically treated garlic cloves survive at lower temperatures than the sham controls.

some other non-magnetic ice nucleating effect became significant. Instead, there is a significant increase in the probability of freezing in the 1 mT rotating fields, followed by a reversal at around 1.5 mT, and then inhibition in fields at 2 mT and above (Fig. 3 and Tables 1, 3).

We suggest that this strange reversal with increasing field strength might have a biochemical basis, as illustrated schematically here in

Fig. 5A–C. Previous work indicates that the ability of plants to supercool may be genetic and heritable[27,37]. Plants that are exposed to sub-freezing temperatures during winter months ought to have evolved methods to inhibit ice nucleation on magnetite nanoparticles within their tissues, possibly with peptides or other molecules designed to block active sites on the crystal surface. Ice nucleation on mineral surfaces typically happens at specific crystallographic locations where some aspect of the local chemical and physical environment facilitates the epitaxial arrangement of water molecules to form seed nuclei (e.g. ref. 38). Garlic has been grown extensively in areas where winter freezing annually penetrates deep into the soil zone where the bulbs are buried[28,29].

Cold-adapted plants that inhabit temperate and high-latitude environments are known to accumulate substances that protect their tissues from frost damage during severe winters. Common solutes are sugars, proline, and glycine betaine, which depress the liquid freezing temperature via changes in osmolarity[39–41]. It is reasonable to suggest that plants living in such environments would also have evolved separate inhibitory mechanisms to reduce the probability of ice nucleation on biological magnetite crystals during hard winter months. Molecules that bind specifically to magnetite crystals to control their morphology have been discovered in the magnetotactic bacteria[42], although it is not yet known if they have any effects on ice nucleation. Identification of magnetite-specific agents in plant tissues and the genes that control their production might allow this ability to be transferred to plant species that are more easily damaged by frost[43], reducing this loss to the human food supply[5,6]. Testing the idea presented here that cold-adapted plants possess epitaxial blocking agents active on nanocrystals of biogenic magnetite might lead to improvement in the technology of plant growth and help reduce the probability of devastating crop failure from frostbite.

Biophysically, the idea that the magnetic oscillations might interfere with the binding of epitaxial surface molecules is plausible. As an order-of-magnitude guide, the magnetostatic potential energy of a particle is given by Eq. (2) above. A single-domain magnetosome ~260 nm in size, as permitted by our magnetometry results, would have a magnetic moment of ~4×10^{-15} A m^2. In a 1 mT field, this would have a maximum magnetostatic potential energy of ~$1000kT$ (where kT is the one-dimensional thermal background energy, k is the Boltzmann constant, and T is the absolute temperature, here taken as the freezing point of water at ~273 K). Because the energies are well above thermal noise, inhibitory proteins attached to the crystal surface could be displaced slightly or even removed, permitting water molecules access to the ice nucleating sites on the magnetite crystals, as indicated schematically in Fig. 5B. This could produce an initial spike in the nucleation probability and a depression of the survivorship curve, as observed in our experiments at 1 and 1.5 mT. At higher field intensities, the particle motions would have larger amplitudes, leading to the direct disruption of water molecule clusters at the crystal surface, as illustrated in Fig. 5C and discussed by Kobayashi et al. [13,17]. Figure 5C1 illustrates this, where both the magnetite-binding substances and incipient ice nucleating clusters are driven away from the agitating surface of the magnetite crystals.

Our primary result that rotating magnetic fields of 2 mT and above significantly inhibit freezing in a living plant is consistent with previous data showing that magnetite is a powerful ice nucleation agent[13,17]. Although the biological function of this magnetite in plants is yet unknown, our data confirm that it is there in trace amounts.

Methods

Deep-freezer system

We followed the method described by Kobayashi et al. [17], diagrammed here in Fig. 1, in which a large Styrofoam box is suspended in the middle of a biomedical grade −80 °C freezer (CLN-35C, Nihon Freezer, Inc.), which cools it from the outside. The inside of this box is warmed with four electric heat pads that are energized under PID control by an external temperature process controller (TPC), initially an Omega model 76000, then replaced by Omron Digital Controller model E5CC). The TPC switched the AC line current on/off through the heating pads via a solid-state relay (SSR),

controlled by a type "T" thermocouple mounted in the bottom center of the coil system. Three small fans mounted on the top, and two sides of the chamber circulated air to reduce vertical temperature gradients. Before each run, the freezer was allowed to tune to a desired equilibrium temperature with the coils set at the required current levels (field or sham).

Magnetic coil system

As also shown in Fig. 1, we used the three-axis set of nested, square Helmholtz coils described by Kobayashi et al. [17], located within the Styrofoam box noted above. All coils were double-wrapped (bi-filar) and wired in series so that a simple DPDT relay system could invert the direction of current flow in one loop, thereby switching the set from actively producing an external magnetic field (active mode, where current in both loops are in the same direction) to one where no external field was generated (sham mode, where adjacent wires had opposite current flow, canceling the external field)[44]. DPDT relay settings, one for each of the three axes, were set by the controlling computer. The two horizontal coils were driven with 10 Hz sine waves programmed to be 90° out of phase (sine and cosine waves), such that it produced a rotating magnetic field vector of constant magnitude in the center of the coil system. These control signals were produced with an Owon® AG1022F dual-channel digital function generator. These voltage signals drove both channels, respectively, of a Crest® model 8200 stereo audio amplifier. We adjusted the amplitudes of the input signals from the Owon® to produce equal peak field strengths for each component of the horizontally rotating vector. To tilt the rotating field at 45° relative to the horizontal, we used a DC power supply to add a downwards-directed magnetic component with the same magnitude as the rotating component. We used an FW Bell® 5180 digital Hall-probe gaussmeter for the calibration of each component so that we could adjust the total intensity of the moving field to the desired level. This field rotation configuration is designed to oscillate magnetite crystals in a fashion that keeps the entire surface of the magnetite crystals in motion relative to the surrounding liquid[17], minimizing the chance of epitaxial ice crystal nucleation. We chose to do our experiments at 0.5 mT steps between 1.0 and 2.5 mT, although the 2.5 mT level required the use of a slightly smaller, double-wrapped coil set (used only for those experiments). Due to the different impedances of the active vs. sham coil settings, the current flow needed to produce these fields was recorded and used to adjust the driving voltages to make the current flowing for the sham control experiments match that of the active ones. Note that the heat dissipated by the coils is a function of the current (I^2R), which is why we matched the current for the paired sham conditions at each field exposure level.

Thermocouple measurements

We used a Measurement Computing Systems® thermocouple module USB-TC, configured with eight thin-wire type T (Cu/Cu–Ni) sensors, which have the manufacturer's estimated accuracy of ±0.25 °C. Two of these sensors monitored the background temperature of the cold chamber on opposite sides of the garlic bulbs, and the others were affixed to the outside of the garlic cloves. To obtain reliable measurements of the temperature of individual cloves, we used thermocouple sensors, which had the thermocouple elements embedded in flat, ~5 mm square thermally resistant plastic tabs. These tabs were taped to the exterior surface of individual garlic cloves within the bulbs and thermally linked to the surface using a small amount of high thermal conductivity paste (Omega™, Omegatherm 201™).

Individual garlic bulbs consisted of bundles of ~5–8 individual cloves, separated from each other by paper-thin, dry layers formed from the sheathing bases of the foliage leaves within which the cloves grow[45]. These onion-like layers of dry skin that separate the cloves are hydrophobic, and hence provide a barrier that prevents ice crystals from one clove, when frozen, from inducing ice nucleation in its neighbors. Hence, each clove provides a statistically independent record of an ice nucleating event that causes that clove to freeze. Each clove in the bulb was numbered with a marking pen corresponding to the digital number of the recording thermocouple, allowing the specific thermal trace from each clove to be matched

with the results of the subsequent viability. For the survivorship analysis, the lowest temperature recorded within two seconds prior to the spikes for cloves experiencing freezing events was used, whereas the final temperature of the run was used for those that did not freeze or did not have thermocouples attached (the 'censored' group).

Cooling data

Once the refrigeration system of the Styrofoam box was tuned to the desired temperature, we lowered a single room-temperature garlic bulb for each experiment into the center of the coil system, suspended by the thermocouple leads as shown schematically in Fig. 1A. Temperatures of individual cloves (thermocouples #1–#6) and the left /right side of the coil background assembly (#7 and #8) were recorded at 2 s intervals on all leads for the 10–20-h duration of each experiment. After each experiment, the clove was warmed, wrapped with newspaper, and stored at 10 °C until it was sent to the National Agriculture and Food Organization (NARO) in Tsukuba for growth analysis. To analyze the data, we checked the thermal record with the individual bulb number corresponding to the digital number of the recording thermocouple. For the sharp thermal pulses on each data channel, we recorded the clove number and the lowest temperature it reached just prior to freezing. For those that did not show the sharp thermal pulses during the whole course, we recorded the final equilibrium temperature that the thermocouples on the garlic bulb reached.

Plant genetic resources

The garlic cultivar 'White' (*Allium sativum* L.) was used in these experiments. Bulbs were raised in Ibaraki prefecture under field conditions and stored at the National Agriculture and Food Research Organization (NARO) in Tsukuba, Japan; they were sent as needed to the Tokyo Institute of Technology over the course of the experiments (9/2020– 2/2022). Given the possibility of slight variabilities in the agricultural product, we tried to balance the ratio of sham vs. field-exposed experiments conducted within each batch, aiming for similar cooling temperatures within the experimental chambers.

Measurement of viability

After completion of each cooling experiment in Tokyo, bulbs were sent promptly to NARO for the viability tests; no information concerning freezing results was provided prior to the viability measurements, ensuring proper blinding. The bulbs of garlic were washed and surface-sterilized with 70% (v/v) ethanol for 5 min and 2% (v/v) sodium hypochlorite solution for 10 min, then rinsed three times in sterilized water. All of the shoot tips (about 2.0 mm long) were excised from the bulbs under a laminar flow hood using a stereomicroscope. Excised shoot tips were placed on solidified ½ strength MS medium[46] with 0.08 M sucrose and 0.8% (w/v) agar, adjusted to pH 5.8 (initial medium) at 25 °C, with a 16-h light/8-h dark photoperiod under a light intensity of 55 μmol m^{-2} s^{-1} provided by LED bar lights for plant growth (standard condition). After exposure experiments regrowth of shoot tips was evaluated after 10 days of re-culture under standard conditions by counting the number of normal shoots developed.

Rock magnetism

Superconducting moment magnetometry using superconducting quantum interference device (SQUID) sensors can detect sub-picogram levels of ferromagnetic materials dispersed in ~10 g samples[15,21,47,48]. In addition, analysis of the coercivity spectrum during magnetization and demagnetization experiments provides constraints on the mineralogy, grain size, and interparticle interaction characteristics[33,47].

At Caltech, we used a vertically oriented 2 G Enterprises™ 3-axis superconducting rock magnetometer[15] with DC-SQUIDS, housed in a magnetically shielded clean laboratory (class 1000), as described previously[17,21,48]. The threshold moment sensitivity of these devices is on the order of 10^{-13} A m^2 (10^{-10} emu, in the Gaussian CGS system). Magnetite's saturation magnetization is 4.8×10^5 A/m (480 emu/cc), so an assemblage of randomly dispersed, immobilized single-domain crystals will produce a

saturation remanent magnetization exactly half of this, or 2.4×10^5 A/m[49]. Hence, the baseline sensitivity of these instruments corresponds to $\sim 4 \times 10^{-13}$ cc of magnetite, or (using magnetite's density of 5.2 g/cc), about 2 pg. This can be distributed anywhere within the ~ 30 cm^3 uniform sense region of the superconducting Helmholtz pickup coils[15]. In practice, this baseline sensitivity is limited by the presence of trace levels of ferromagnetic contaminants in the objects holding the sample to be measured[48]. We, therefore, used a thin monofilament fishing line, soaked overnight in 6 N HCl to leach out contaminants, with slip knots tied at each end to support the sample. Saturation isothermal remanent moments of these threads are below the instrument measurement threshold.

Four whole garlic bulbs from the collections being measured in Tokyo were frozen on dry ice and transported as carry-on baggage to the clean-lab facility at Caltech (US Department of Agriculture importation permit #A-00083351, 12/21/2021). Using only utensils and surfaces in the clean lab that had been washed in 6 N HCl, individual cloves from these bulbs were removed using ceramic knives (Kyocera™), stripped of the external sheaths (which might have picked up external contaminants), and mounted on the monofilament strings using slip-knots. The sample access region of the magnetometer was cooled to about -30 °C using a steady flow of dry nitrogen gas that was passed through a 0.2 μm filter. This gas was then chilled by passing it through a coiled tube in a 10-l liquid nitrogen Dewar and plumbed into the bottom of the sample access port of the magnetometer. Gas flowing out the top of the magnetometer was checked periodically by a portable laser particle counter (MetOne™) and confirmed to be less than class 100 (e.g., less than 10 particles larger than 0.3 μm per cubic foot were detected).

After suspension on a clean monofilament fiber, individual cloves were held for ~ 10 min in the cold stream of N$_2$ gas in the magnetometer access port to freeze them solid, thereby immobilizing any ferromagnetic particles that might be present. The temperature of the N$_2$ gas flow was monitored using a non-magnetic fiber optic thermal sensing system (Omega®, Inc.), for which the fiber sensors were positioned inside the vertical sense region of the magnetometer. We then subjected them to a series of experiments designed to measure their domain state (single-domain vs. multi-domain), their coercivity spectra (which provide constraints on the mineralogy and average particle volume and shape), as well as how they are spatially arranged (isolated, or grouped in clumps). In order, these experiments were: (1) The progressive acquisition of an anhysteretic remanent magnetization, acquired by exposing the sample to a 100 mT peak oscillating magnetic field at about 1 kHz, in the presence of a controlled DC biasing (offset) field increasing in 0.1 mT steps between 0 and 1 mT. This provides a measure of how the particles are spatially arranged (isolated or in clumps)[33,47]. (2) The maximum ARM was then progressively demagnetized in alternating fields (Afs) in a zero background at peak oscillating field strengths up to 100 mT and paired with the demagnetization pattern of a similar, single 100 mT magnetic pulse (an Isothermal Remanent Magnetization, or IRM). This pair of curves provides the ARM equivalent of the Lowrie-Fuller test of domain state, to distinguish single-domain from multi-domain particles[35,36]. (3) To constrain the magnetic mineralogy, determine the coercivity spectra, and test for interactions, the sample was subjected to a series of progressive increasing IRM pulses, followed by progressive AF demagnetization as described by Cisowski[33]. Constraints on the mean particle size were estimated from Fig. 3 of Diaz-Ricci and Kirschvink[34], assuming the most equant particle shape for ellipsoidal solids that match the measured mean coercivity. (4), Finally, using a superconducting Quantum Design™ Magnetic Properties Measurement System (MPMS-XL5), we conducted a warming remanence series from 5 to 300 K on a commercially sourced garlic clove to test for the Verwey transition, which is a definitive test for the presence of magnetite.

Statistics and reproducibility

As noted above, Table 1 shows the statistical comparison of field exposure vs. survival for all 127 garlic bulbs (and the 721 cloves) that were used for the experiments, as well as the replicate numbers in each group. Precise data are given in the Supplementary Data 1 file. Bulbs were sent from the Kobayashi group in Meguro to the Tanaka group in Tsukuba in a blinded fashion for the viability assay, without identifying the magnetic treatment or results. The simplest statistical test is, therefore, a series of 2×2 contingency tables (Alive/Dead vs. Field/Sham) for the four field levels used (1.0, 1.5, 2.0, and 2.5 mT), which can individually be analyzed via the classical Pearson's[50] χ^2 test. This is justified, given the large number of observations and the temporal independence of freezing events. This temporal independence is predicted by the dry, hydrophobic foliage leaves that surround each garlic clove, providing a physical barrier that stops ice from penetrating from outside. To test the hypothesis of consistent differences, we used the Cochran–Mantel–Haenszel test for repeated tests of independence as described in Ch. 2.10 of McDonald[51], using the linked spreadsheet for analysis.

Concerning the survivorship statistics, we note that the temperature/freezing data generated by the monitored cooling of garlic cloves yields a data set similar in principle to the commonly used 'survivorship' analysis in biomedical studies. Those studies measure the fraction of a population remaining as a function of time after a treatment or control starts, with a record of events like death or failure vs. time as the outcome. Kaplan and Meier[31] originally suggested a quantitative method to place statistical constraints on the fraction of a population surviving as a function of time, and this has been expanded into a major branch of statistics[52]. Although our experiments monitor the freezing events as a function of decreasing temperature instead of increasing time, we note that existing modifications of the Kaplan–Meier statistics are adequate to adjust for the highly non-linear physical chemistry of ice nucleation.

In our study the temperature values are negative and generally decreasing (except for exothermic pulses when supercooled cloves freeze). Hence, we convert our temperature data to positive numbers ($-T$). All cloves were scored as to viability after exposure to low temperatures. Hence, we grouped the survivorship distribution function into three types of data as follows:

'Exactly Observed' observations are those for which a garlic clove froze, and there was a thermocouple mounted on it which recorded the temperature spike from the release of the latent heat of crystallization of the water (~ 80 cal/g). The lowest temperature reached before the spike is analogous to the time of a recorded death event in a standard survivorship analysis, except ($-$) temperature is used rather than time. These are analogous to patients who died during a survivorship study. A clove that froze at -9.5 °C with a thermocouple on it would be 'Exactly Observed', and the matrix entry for it would be (9.5, 9.5).

'Right-Censored' observations are garlic cloves that did not freeze or die during the sub-freezing exposure interval, and this category includes both the set of surviving cloves that did and those that did not have thermocouples. We know the minimum temperature to which they survived from the average of the sensors attached to the whole garlic bulb. These are analogous to patients who survived a survivorship study. An 'Interval Censored' clove that froze without a sensor on it that reached a temperature of -12.5 °C would be entered as (2.7, 12.5); this is the interval in which the event could have happened given the maximum freezing temperature.

'Interval-Censored' observations are those in which the garlic clove did not have a thermocouple on it, but it was dead after the experiment. It most likely died sometime between the melting temperature of garlic (known to be at -2.7 °C)[27] and the minimum temperature that the chamber reached, as recorded by the thermocouples. A 'Right-Censored' clove that survived an experiment that reached -11.5 °C would be entered as (11.5, Inf), where the 'Inf' parameter is a flag to tell the software that the clove survived to this point, and no further information is available.

These data are comparable to results from a biomedical survivorship survey in which a patient in one of the groups died, but the exact time of death is unknown. Although these data are useful for constraining the shape of the freezing vs. temperature curves, the problem of how to incorporate them into the statistical comparison of two curves, which needs a 'robust

variance' is yet an unresolved problem[53,54]. We used Kaplan–Meier analyses[31] for the exact observed and right-censored data using the R-language statistical server program, "survival"[54,55], and visualized with "survminer"[56]. The log-rank test is a nonparametric test to compare the two-survival distribution, Kaplan–Meier analysis. However, as the probability of heterogeneous freezing on an ice nucleating particle is a highly non-linear function with temperature[57], the standard log-rank tests are inappropriate. We, therefore, use the Mann–Whitney–Wilcoxon test, which is also known as the Wilcoxon rank-sum test, which does not assume a uniform probability distribution of the events being analyzed. We implemented this using the Survival, Survminer, and Interval packages in the R language[58]. Data are entered as a $3 \times N$ matrix, where N is the number of observations, and the values are pairs of the bounding temperature or a bounding flag. The sham and field data were combined in one dataset. Columns 1 and 2 are the same as in the Kaplan–Meier analyses described in the previous paragraph. To distinguish the field and the sham data, column 3 was added in which 0 corresponds to the field data and 1 indicates the sham data.

Data availability

The first tab of the appended Excel file (Supplementary Data 1) gives the cooling, freezing, and viability data for all garlic bulbs and cloves from this study. Subsequent tabs show the data organization for Tables 1–3, the associated statistical tests, and source data for charts presented in the main figures. This file is available online or from the senior author.

References

1. Macdonald, F. A. et al. Calibrating the cryogenian. *Science* **327**, 1241–1243 (2010).
2. Fischer, A. G. in *Climate in Earth History: Studies in Geophysics* Vol. 9 (ed. National Research Council) 97–104 (The National Academies Press, 1982).
3. Rubinstein, C. V., Gerrienne, P., de la Puente, G. S., Astini, R. A. & Steemans, P. Early Middle Ordovician evidence for land plants in Argentina (eastern Gondwana). *N. Phytol.* **188**, 365–369 (2010).
4. Sakai, A. & Larcher, W. *Frost Survival of Plants: Responses and Adaptation to Freezing Stress* Vol. 62 (Springer, Berlin, Heidelberg, 1987).
5. Gunders, D. *Wasted: How America is Losing up to 40 percent of its Food from Farm to Fork to Landfill*. Natural Resources Defense Council Issue Paper IP, 12-06-12-0 (2012).
6. Gunders, D. et al. *Wasted: How America is Losing Up to 40 Percent of Its Food from Farm to Fork to Landfill*. 2nd edn. NRDC's Original 2012 Report. Issue Paper IP 17-05-17-0 (Natural Resources Defense Council, 2017).
7. Hoshino, T., Odaira, M., Yoshida, M. & Tsuda, S. Physiological and biochemical significance of antifreeze substances in plants. *J. Plant Res.* **112**, 255–261 (1999).
8. Moore, E. B. & Molinero, V. Structural transformation in supercooled water controls the crystallization rate of ice. *Nature* **479**, 506–508 (2011).
9. Lowenstam, H. A. & Weiner, S. *On Biomineralization* (Oxford University Press, 1989).
10. Marcolli, C., Nagare, B., Welti, A. & Lohmann, U. Ice nucleation efficiency of AGI: review and new insights. *Atmos. Chem. Phys.* **16**, 8915–8937 (2016).
11. Cochet, N. & Widehem, P. Ice crystallization by *Pseudomonas syringae*. *Appl. Microbiol. Biotechnol.* **54**, 153–161 (2000).
12. Atkinson, J. D. et al. The importance of feldspar for ice nucleation by mineral dust in mixed-phase clouds. *Nature* **498**, 355–358 (2013).
13. Kobayashi, A., Golash, H. N. & Kirschvink, J. L. A first test of the hypothesis of biogenic magnetite-based heterogeneous ice-crystal nucleation in cryopreservation. *Cryobiology* **72**, 216–224 (2016).
14. Kobayashi, A. & Kirschvink, J. L. A ferromagnetic model for the action of electric and magnetic fields in cryopreservation. *Cryobiology* **68**, 163–165 (2014).
15. Fuller, M., Goree, W. S. & Goodman, W. L. in *Magnetite Biomineralization and Magnetoreception in Organisms: A New Biomagnetism* Vol. 5 *Topics in Geobiology* (eds Kirschvink, J. L., Jones, D. S. & MacFadden, B. J.) 103–151 (Plenum Press, 1985).
16. Butler, R. F. & Banerjee, S. K. Theoretical single-domain size range in magnetite and titanomagnetite. *J. Geophys. Res.* **80**, 4049–4058 (1975).
17. Kobayashi, A., Horikawa, M., Kirschvink, J. L. & Golash, H. N. Magnetic control of heterogeneous ice nucleation with nanophase magnetite: Biophysical and agricultural implications. *Proc. Natl Acad. Sci. USA* **115**, 5383–5388 (2018).
18. Wowk, B. Electric and magnetic fields in cryopreservation. *Cryobiology* **64**, 301–303 (2012). author reply 304–305.
19. Mann, S., Sparks, N. H., Walker, M. M. & Kirschvink, J. L. Ultrastructure, morphology and organization of biogenic magnetite from sockeye salmon, *Oncorhynchus nerka*: implications for magnetoreception. *J. Exp. Biol.* **140**, 35–49 (1988).
20. Kirschvink, J. L., Jones, D. S. & McFadden, B. J. *Magnetite Biomineralization and Magnetoreception in Organisms: A New Biomagnetism* Vol. 5 (Plenum Press, 1985).
21. Kirschvink, J. L., Kobayashi-Kirschvink, A. & Woodford, B. J. Magnetite biomineralization in the human brain. *Proc. Natl Acad. Sci. USA* **89**, 7683–7687 (1992).
22. Bazylinski, D. A. & Frankel, R. B. Magnetosome formation in prokaryotes. *Nat. Rev. Microbiol.* **2**, 217–230 (2004).
23. Leao, P. et al. Magnetosome magnetite biomineralization in a flagellated protist: evidence for an early evolutionary origin for magnetoreception in eukaryotes. *Environ. Microbiol.* **22**, 1495–1506 (2019).
24. Gajdardziska-Josifovska, M., McClean, R. G., Schofield, M. A., Sommer, C. V. & Kean, W. F. Discovery of nanocrystalline botanical magnetite. *Eur. J. Mineral.* **13**, 863–870 (2001).
25. Chaffee, T. M., Kirschvink, J. L. & Kobayashi, A. in *AGU Fall meeting 2015* GP51A-1308 (American Geophysical Union, San Francisco, CA, 2015).
26. Gorobets, Y., Gorobets, S., Gorobets, O., Magerman, A. & Sharai, I. Biogenic and anthropogenic magnetic nanoparticles in the phloem sieve tubes of plants: magnetic nanoparticles in plants. *J. Microbiol. Biotechnol. Food Sci.* **12**, e5484 (2023).
27. James, C., Seignemartin, V. & James, S. J. The freezing and supercooling of garlic (*Allium sativum* L.). *Int. J. Refrig.* **32**, 253–260 (2009).
28. Rivlin, R. S. Historical perspective on the use of garlic. *J. Nutr.* **131**, 951S–954S (2001).
29. Petrovska, B. B. & Cekovska, S. Extracts from the history and medical properties of garlic. *Pharmacogn. Rev.* **4**, 106–110 (2010).
30. Liu, K. et al. Janus effect of antifreeze proteins on ice nucleation. *Proc. Natl Acad. Sci. USA* **113**, 14739–14744 (2016).
31. Kaplan, E. L. & Meier, P. Nonparametric estimation from incomplete observations. *J. Am. Stat. Assoc.* **53**, 457–481 (1958).
32. Thompson, R. & Oldfield, F. *Environmental Magnetism* XII, Vol. 228 (Springer, Dordrecht, 1986).
33. Cisowski, S. Interacting vs. non-interacting single-domain behavior in natural and synthetic samples. *Phys. Earth Planet. Int.* **26**, 56–62 (1981).
34. Diaz Ricci, J. C. & Kirschvink, J. L. Magnetic domain state and coercivity predictions for biogenic greigite (Fe$_3$S$_4$): a comparison of theory with magnetosome observations. *J. Geophys. Res.* **97**, 17309–17315 (1992).
35. Lowrie, W. & Fuller, M. On the alternating field demagnetization characteristics of multidomain thermoremanent magnetization in magnetite. *J. Geophys. Res.* **76**, 6339–6349 (1971).

36. Johnson, H. P., Lowrie, W. & Kent, D. V. Stability of ARM in fine and course grained magnetite and maghemite particles. *Geophys. J. R. Astron. Soc.* **41**, 1–10 (1975).

37. Fuller, M. P., White, G. G. & Charman, A. The freezing characteristics of cauliflower curd. *Ann. Appl. Biol.* **125**, 179–188 (1994).

38. Holden, M. A., Campbell, J. M., Meldrum, F. C., Murray, B. J. & Christenson, H. K. Active sites for ice nucleation differ depending on nucleation mode. *Proc. Natl Acad. Sci. USA* **118**, e2022859118 (2021).

39. Uemura, M. & Kamata, T. Role of intracellular compatible solutes in cold acclimation in plants (in Japanese). *Cryobiol. Cryotechnol.* **47**, 49–50 (2001).

40. Steponkus, P. L. Role of the plasma membrane in freezing injury and cold acclimation. *Annu. Rev. Plant Physiol.* **35**, 543–584 (1984).

41. Levitt, J. *Responses of Plant to Environmental Stress: Water, Radiation, Salt and Other Stresses* (Academic Press, 1980).

42. Pohl, A. et al. Magnetite-binding proteins from the magnetotactic bacterium *Desulfamplus magnetovallimortis* BW-1. *Nanoscale* **13**, 20396–20400 (2021).

43. Wisniewski, M. et al. in *Plant Cold Hardiness: Gene Regulation and Genetic Engineering* Vol. 15 (eds Li, P. H. & Palva, E. T.) 211–221 (Kluwer Academic/lenum Publishers, 2002).

44. Kirschvink, J. L. Uniform magnetic fields and double-wrapped coil systems: improved techniques for the design of biomagnetic experiments. *Bioelectromagnetics* **13**, 401–411 (1992).

45. Mann, L. K. Anatomy of the garlic bulb and factors affecting bulb development. *Hilgardia* **21**, 194–251 (1952).

46. Murashige, T. & Skoog, F. A revised medium for rapid growth and bioassays with tobacco tissue cultures. *Physiol. Plant.* **15**, 473–497 (1962).

47. Kobayashi, A. et al. Experimental observation of magnetosome chain collapse in magnetotactic bacteria: sedimentological, paleomagnetic, and evolutionary implications. *Earth Planet. Sci. Lett.* **245**, 538–550 (2006).

48. Kirschvink, J. L., Kopp, R. E., Raub, T. D., Baumgartner, C. T. & Holt, J. W. Rapid, precise, and high-sensitivity acquisition of paleomagnetic and rock-magnetic data: development of a low-noise automatic sample changing system for superconducting rock magnetometers. *Geochem. Geophys. Geosyst.* **9**, n/a-n/a (2008).

49. Butler, R. F. *Paleomagnetism: Magnetic Domains to Geologic Terranes* (Blackwell Scientific Publications, 1992).

50. Pearson, K. X. On the criterion that a given system of deviations from the probable in the case of a correlated system of variables is such that it can be reasonably supposed to have arisen from random sampling. *Lond. Edinb. Dublin Philos. Mag. J. Sci.* **50**, 157–175 (1900).

51. Zimmermann, F. et al. Ice nucleation properties of the most abundant mineral dust phases. *J. Geophys. Res.: Atmos.* **113**, D23204-1,11 (2008).

52. Kalbfleisch, J. D. & Prentice, R. L. *The Statistical Analysis of Failure Time Data* 2nd edn (John Wiley & Sons, 2002).

53. Karadeniz, P. G. & Ercan, I. Examining tests for comparing survival curves with right censored data. *Stat. Transit. N. Ser.* **18**, 311–328 (2017).

54. Therneau, T. M. et al. *A Package for Survival Analysis in R* https://CRAN.R-project.org/package=survival (2023).

55. Therneau, T. M. & Grambsch, P. M. *Modeling Survival Data: Extending the Cox Model. [Electronic Resource]* (Springer, New York, 2000).

56. Kassambara, A. et al. Survminer: *Drawing Survival Curves Using 'ggplot2' v. 2021-03-09* (GitHub, 2021).

57. Vali, G. Interpretation of freezing nucleation experiments: singular and stochastic; sites and surfaces. *Atmos. Chem. Phys.* **14**, 5271–5294 (2014).

58. Fay, M. P. & Shaw, P. A. Exact and asymptotic weighted logrank tests for interval censored data: the interval R package. *J. Stat. Softw.* **36**, i02 (2010).

Acknowledgements

Author contributions

Conceptualization: A.K. Methodology: A.K., J.L.K., K.S., D.T., H.H., and T.K. Investigation: D.T., A.K., H.H., K. Kawai, T.K., J.L.K. Visualization: K.S., J.L.K., A.K. Supervision: A.K. Writing—original draft: A.K., J.L.K., K. Kihara. Writing—review & editing: A.K., J.L.K., K. Kihara, and K.S.

Competing interests

The authors declare no competing interests.

Additional information

Supplementary information The online version contains supplementary material available at https://doi.org/10.1038/s42003-024-06749-7.

Correspondence and requests for materials should be addressed to Atsuko Kobayashi, Daisuke Tanaka or Joseph L. Kirschvink.

Peer review information *Communications Biology* thanks the anonymous reviewers for their contribution to the peer review of this work. Primary Handling Editors: Huijuan Guo and David Favero. A peer review file.

Reprints and permissions information is available at http://www.nature.com/reprints

Publisher's note Springer Nature remains neutral with regard to jurisdictional claims in published maps and institutional affiliations.